N-6-methyladenosine (m6A) Promotes the Nuclear Retention of mRNAs with Intact 5' Splice Site Motifs

Eliza S. Lee[1,5], Harrison. W. Smith[1], Sean S. J. Ihn[1], Leticia Scalize de Olivera[1], Yifang E. Wang[1], Robert Y. Jomphe[1,2], Syed Nabeel-Shah[3,4], Shuye Pu[4], Jack F. Greenblatt[3,4], Alexander F. Palazzo[1,6]

1- **University of Toronto, Department of Biochemistry, Canada**

2- **Cell Biology Program, Hospital for Sick Children, Toronto, Canada**

3- **University of Toronto, Department of Molecular Genetics, Canada**

4- **Terrence Donnelly Centre for Cellular & Biomolecular Research, Toronto, Canada**

5- **Present Address: Department of Biochemistry, University of Colorado Boulder, CO**

6- **Corresponding author**

Abstract

In eukaryotes, quality control of mRNA represents an important regulatory mechanism for gene expression. Misprocessed mRNAs that contain an intact 5' Splice Site (5'SS) motif are retained in the nucleus and targeted for decay. Previously, we showed that the nuclear retention of these transcripts requires ZFC3H1, a component of the Poly(A) Exosome Targeting (PAXT) complex, and U1-70K, a component of the U1 snRNP. In *S. pombe*, the ZFC3H1 homolog, Red1, binds to the YTH-domain containing protein Mmi1 to target certain RNA transcripts for nuclear retention and decay. Here we show that ZFC3H1 and U1-70K interact with YTHDC1 and YTHDC2, two YTH domain-containing proteins that bind to N-6-methyladenosine (m6A) modified RNAs. We then show that YTHDC1 and YTHDC2 are required for the nuclear retention of mRNAs with intact 5'SS motifs. Furthermore, disruption of m6A methyltransferase activity inhibits the nuclear retention of these transcripts. Using m6A-miCLIP analysis, we map m6A methylation marks to intronic polyadenylated (IPA) transcripts, which contain intact 5'SS motifs and are nuclear retained and degraded in a ZFC3H1-dependent manner. We find that m6A is enriched near intact 5'SS motifs and the poly(A)-tail. Overall, this work suggests that the m6A modification acts as part of an evolutionarily conserved quality control mechanism that targets misprocessed mRNAs for nuclear retention and decay.

Introduction

Eukaryotic cells are divided into two compartments: the nucleus where pre-mRNAs are synthesized and processed, and the cytoplasm where mature mRNAs are translated into proteins. This subcellular division allows for extensive quality control at the level of both RNA synthesis and RNA processing (Palazzo and Lee 2018; Garland and Jensen 2020). These quality control pathways promote the nuclear retention and degradation of spurious transcripts and misprocessed mRNAs and thus preventing them from accessing the translation machinery in the cytoplasm. Importantly, misprocessed mRNAs typically retain RNA processing *cis*-elements which then target the mRNA for retention and decay (Legrain and Rosbash 1989; Abad et al. 2008; Lee et al. 2015).

One class of misprocessed mRNAs are intronic polyadenylated (IPA) transcripts (Tian et al. 2007). These are generated by cryptic 3'cleavage/polyadenylation signals found in introns. Although most cryptic 3'cleavage/polyadenylation signals in introns are suppressed (Kaida et al. 2010), they can be used at low levels to generate IPAs that tend to encode protein fragments (Ogami et al. 2017). These are often toxic as they can compete with endogenous proteins for their binding partners (Veitia 2007). IPA transcripts contain intact 5' splice site (5'SS) motifs, which are present at the boundary between the upstream exon and the intron where the 3'cleavage occurs. We and others have shown that the presence of an intact 5'SS motif in an RNA promotes its nuclear retention and decay (Legrain and Rosbash 1989; Abad et al. 2008; Lee et al. 2015). These transcripts are recognized by the U1 snRNP, and our group and others have previously shown that the U1 component U1-70K is required for their nuclear retention and decay (Fortes et al. 2003; Abad et al. 2008; Goraczniak et al. 2009; Lee et al. 2022). We also found that U1-70K associates with ZFC3H1, a component of the Poly(A) Exosome Targeting (PAXT) complex (Lee et al. 2022). PAXT also contains the nuclear poly(A) binding protein, PABPN1, and the RNA helicase MTR4,

which is known to feed RNAs into the nuclear exosome, the major RNase complex in human cells (Meola et al. 2016; Ogami et al. 2017; Ogami and Manley 2017; Silla et al. 2018, 2020). The PAXT complex promotes the degradation of many types of polyadenylated RNAs, including mRNAs, non-coding RNAs (ncRNAs) and spurious transcripts associated with pervasive transcription. We and others showed that ZFC3H1 is required for the nuclear retention and decay of RNAs with intact 5'SS motifs including IPA transcripts (Ogami et al. 2017; Lee et al. 2022). Interestingly, we found that MTR4 was not required for the nuclear retention of these RNAs (Lee et al. 2022), although it has been reported to inhibit the recruitment of the RNA export factor ALYREF to RNAs (Fan et al. 2017). We also observed that the depletion of PABPN1 did not significantly affect the nuclear retention of RNAs with intact 5'SS motifs, however it inhibited nuclear mRNA export (Lee et al. 2022) as reported by others (Apponi et al. 2010). As inhibition of mRNA export typically enhances the nuclear retention of RNAs with intact 5'SS motifs (Lee et al. 2020), it is possible that PABPN1 contributes to their nuclear retention but that this effect is masked by the general repression of mRNA export in PABPN1-depleted cells.

We previously reported that the intact 5'SS motif targets RNAs to nuclear speckles (Lee et al. 2022), where post-transcription splicing is thought to be performed (Dias et al. 2010). However, due to the lack of a corresponding 3' splice site in these transcripts, U2 snRNP fails to be recruited. Instead, these RNAs acquire ZFC3H1, which inhibits their egress from nuclear speckles and thereby inhibits nuclear export (Lee et al. 2022). Importantly, the over-expression of GFP-CLK3, which disrupts nuclear speckles, inhibited nuclear retention of transcripts with intact 5'SS motifs (Lee et al. 2022).

The PAXT complex is conserved between humans and *S. pombe*, where it is known as the MTREC (Mtl1-Red1 Core) complex, and is composed of Mtl1, the paralogue of Mtr4, Red1, the

paralogue of ZFC3H1 and Pab2, a poly(A) binding protein (Sugiyama and Sugioka-Sugiyama 2011; Zhou et al. 2015; Shichino et al. 2020). MTREC promotes the nuclear retention and decay of meiotic mRNAs that are inappropriately synthesized in interphase cells. MTREC is recruited to these RNAs through a complex of three proteins consisting of Erh1, Pir1 and Mmi1 (Sugiyama and Sugioka-Sugiyama 2011; Sugiyama et al. 2016; Wei et al. 2021; Shichino et al. 2020). Mmi1 contains a YTH domain which in other systems recognizes m6A modified RNAs. However in *S. pombe*, no m6A is detectable in mRNAs (Ishigami et al. 2021) and instead the YTH domain of Mmi1 binds to determinant-of-selective-removal RNA elements found in meiotic mRNAs (Chen et al. 2011; Sugiyama and Sugioka-Sugiyama 2011; Wang et al. 2016). Although humans contain homologues to Erh1 (ERH) and Mmi1 (YTH-proteins as discussed below), there is no clear Pir1 homologue, although it does have a Serine/Proline-rich region that shows a limited homology with the N-terminus of ZFC3H1 (Wei et al. 2021). MTREC and Mmi1 are also involved in the nuclear retention and decay of ncRNAs and transposable element-derived RNAs (Sugiyama et al. 2016; Vo et al. 2019; Zhou et al. 2015). When RNA decay is inhibited, MTREC-targeted RNAs accumulate in a Mmi1/Red1-enriched nuclear foci (Sugiyama and Sugioka-Sugiyama 2011; Shichino et al. 2018, 2020) which are reminiscent of nuclear speckles and/or other nuclear foci implicated in mRNA decay (Silla et al. 2018; Wang et al. 2021).

In humans, YTH domains recognize *N*-6-methyladenosine (m6A) modified of RNAs (Xu et al. 2014). This modification is dynamic and enriched in several regions of mRNAs, including the 5'UTR, the region surrounding the stop codon and the 3' UTR (Dominissini et al. 2012; Meyer et al. 2012), but is depleted around exon-exon junctions (Yang et al. 2022; Uzonyi et al. 2023; He et al. 2023), and as such tends to be enriched in very large exons. The m6A modification is catalyzed by the METTL3 methyltransferase, which forms a complex with METTL14 and other

factors (Liu et al. 2014). This modification can be removed by the demethylases ALKBH5, FTO and perhaps ALKBH3 (Jia et al. 2011; Zheng et al. 2013; Ueda et al. 2017). m6A is predominantly recognized by five YTH domain containing proteins in humans. These include YTHDC1 and YTHDC2, which are predominantly nuclear, and YTHDF1, YTHDF2, and YTHDF3, which are predominantly cytoplasmic (Xu et al. 2021). Initial studies indicated that m6A, and m6A-binding proteins promote mRNA export (Roundtree et al. 2017; Zheng et al. 2013; Lesbirel et al. 2018; Lesbirel and Wilson 2019), however, more recent work analyzing features that impact the flow of RNAs between various compartments by machine learning have found that the levels of m6A modification correlate with nuclear retention (Smalec et al. 2022).

Proteins that add or remove m6A methylation marks have also been linked to nuclear speckles (Jia et al. 2011; Liu et al. 2014; Zheng et al. 2013). YTHDC1 form nuclear foci that partially colocalize with nuclear speckles (Cheng et al. 2021; Nayler et al. 2000) and the depletion of ALKBH5 has been reported to disrupt nuclear speckles (Zheng et al. 2013). YTHDC1 also has the propensity to phase separate and this is potentiated by the presence of RNA (Cheng et al. 2021). m6A and YTHDC1 are also required for the suppression of RNAs generated from transposable elements, enhancer RNAs and other ncRNAs (Liu et al. 2020), reminiscent of the function of MTREC and Mmi1 in *S. pombe*.

Here we show that m6A modification is required for the efficient nuclear retention of mRNAs that contain intact 5'SS motifs, which are found in IPA transcripts. We show that YTHDC1 and YTHDC2 associate with both ZFC3H1 and U1-70K. We find that m6A peaks are enriched in IPAs and accumulate both near the near 5'SS motif and the poly(A)-tail. Our findings indicate that the core components of nuclear surveillance systems, and their ability to functionally interact with one another, are conserved between yeast and humans. Furthermore, our data suggest that m6A

methylation acts as an additional layer of quality control, which in conjunction with other signals, such as intact 5'SS motifs, prevents the nuclear export and promotes the decay of non-functional and misprocessed RNAs.

Results

YTHDC1 and YTHDC2 interacts with both ZFC3H1 and U1-70K

In *S. pombe*, the MTREC associates with Mmi1, a nuclear YTH domain-containing protein (Figure 1A, left) (Sugiyama and Sugioka-Sugiyama 2011; Chen et al. 2011; Zhou et al. 2015; Shichino et al. 2020). To determine whether components of the equivalent human complex (known as PAXT, Figure 1A right) interact with nuclear YTH domain-containing proteins, we expressed either FLAG-HA-YTHDC1 or FLAG-ZFC3H1 (1-1233) in HEK293 cells and assessed their binding partners by co-immunoprecipitation. Note that although the ZFC3H1 fragment used in our experiments is missing amino acids 1234-1989 of the endogenous protein, it contains all of the regions known to participate in protein-protein interactions (Wang et al. 2021). When we probed FLAG-HA-YTHDC1 immunoprecipitates, we could detect both endogenous ZFC3H1 and U1-70K, even in the presence of RNase (Figure 1B-C). In contrast, RNase treatment greatly reduced the co-immunoprecipitation of eIF4AIII (Figure 1B), a component of the exon junction complex (Shibuya et al. 2004). The FLAG-HA-YTHDC1 immunoprecipitates also contained YTHDC2 but not any detectable ALKBH5 or ALY (Figure 1B-C). None of these proteins were detectable in immunoprecipitates from cells not expressing FLAG-HA-YTHDC1. When we probed FLAG-ZFC3H1 (1-1233) immunoprecipitates, we could detect both endogenous YTHDC1 and YTHDC2 in the presence of RNase (Figure 1D-E). In agreement with our previous findings (Lee et al. 2022), we also detected U1-70K in these precipitates. None of these proteins were significantly present in immunoprecipitates from cells not expressing the FLAG-ZFC3H1 fragment. In addition, there was no detectable ALKBH5, eIF4AIII, METTL3 or ALY in the FLAG-ZFC3H1 (1-1233) precipitates.

These results indicate that nuclear YTH proteins associate with ZFC3H1 and U1-70K, two factors required for the nuclear retention of RNAs that contain intact 5'SS motifs, such as IPA transcripts.

DRACH motifs are required for the efficient nuclear retention of 5'SS motif containing reporter mRNAs

The m6A methyltransferase preferentially modifies RNAs at consensus DRACH motifs (G/A/U, A/G, A, C, A/U/C) (Meyer et al. 2012; Dominissini et al. 2012). To test whether m6A was required for nuclear retention, we mutated but of one of the DRACH motifs in the *fushi-tarazu* (*ftz*) reporter which we previously used to study the effect of the 5'SS motif on nuclear retention (Lee et al. 2015). Note that we used an intronless (Δi) version for these studies. For the parental *ftz* reporter (*ftz-Δi*) we identified nine putative DRACH motifs and for the 5'SS motif containing version (*ftz-Δi-5'SS*) we found eleven motifs (Figure 2A). We mutated all the DRACH sites to generate two other reporters, *no-m6A-ftz-Δi* and *no-m6A-ftz-Δi-5'SS* respectively. Note that the consensus 5'SS motif (AAGGUAAGC) was not altered. We expressed these various versions of the *ftz* reporters into human osteosarcoma cell lines (U2OS), and visualized RNA localization by RNA fluorescent in situ (FISH) hybridization using probes that recognize the *ftz* reporter RNA. Consistent with our previous reports, we found that *ftz-Δi* mRNA was efficiently exported whereas *ftz-Δi-5'SS* was nuclear retained (Figure 2B-C). Elimination of the DRACH motifs in *ftz-Δi* had no effect on its distribution (compare *ftz-Δi* to *no-m6A-ftz-Δi*; Figure 2B-C). In contrast, elimination of the DRACH motifs in *ftz-Δi-5'SS*, inhibited its nuclear retention (compare *ftz-Δi-5'SS* to *no-m6A-ftz-Δi*). Indeed, *no-m6A-ftz-Δi* and *no-m6A-ftz-Δi-5'SS*, were both found in the

cytoplasm to the same extent suggesting that the ability of the 5'SS motif to promote nuclear retention was completely abrogated by the removal of DRACH motifs.

We also expressed versions of *ftz-Δi* and *ftz-Δi-5'SS* mRNA with optimized DRACH motifs (AGACT) to enhance methylation (creating *e-m6A-ftz-Δi* and *e-m6A-ftz-Δi-5'SS*; Figure 2A). We only observed a slight increase in nuclear retention of these mRNAs compared to the parental constructs (Figure 2C).

Overall, these results indicate that consensus m6A modification motifs are required for the 5'SS motif to promote efficient nuclear retention of a reporter mRNA. In contrast, the presence or absence of consensus m6A modification motifs did not significantly affect the distribution of a well exported mRNA reporter.

m6A does not affect nuclear speckles targeting of 5'SS motif containing RNAs

Previously, we found that 5'SS motif containing RNAs are targeted and then retained in nuclear speckles (Lee et al. 2015, 2022). ZFC3H1 and U1-70K are dispensable for this targeting but instead are required to inhibit egress of these RNAs out of the nuclear speckles (Lee et al. 2022). Given that many m6A machinery components are localized to nuclear speckles, we asked if the m6A modification promotes targeting of mRNAs into these sub-nuclear structures. To determine the localization of mRNAs at early time points post-synthesis, plasmids containing *ftz-Δi-5'SS* and *no-m6A-ftz-Δi-5'SS* reporter genes were microinjected into the nuclei of U2OS cells to allow for rapid synchronous expression. After allowing for one hour of mRNA expression, a time point when nuclear speckle targeting is highest (Akef et al. 2013), cells were fixed and immunostained for SC35, a nuclear speckle marker (Spector et al. 1991) and probed for *ftz* mRNA

by FISH. We observed robust nuclear speckle targeting of both constructs (Figure 2D-E). This result indicates that within the context of *ftz-Δi-5'SS*, m6A was not required for nuclear speckle targeting. It is possible that m6A methylation promotes targeting to nuclear speckles, but acts redundantly with other RNA elements such as exonic splicing enhancers (Wang et al. 2018).

Next, we assessed whether m6A affected the egress of RNAs containing 5'SS out of nuclear speckles by assessing the colocalization of the reporters and SC35 in transfected cells. In this circumstance, mRNA distribution reaches a steady state and nuclear speckle localization is dictated by the rate of entry and egress. As we previously reported, *ftz-Δi-5'SS* was localized in part to nuclear speckles at steady state (Figure 2F-G). Surprisingly, we observed a slight but consistent colocalization of *no-m6A-ftz-Δi-5'SS* mRNAs with nuclear speckles despite the fact that the mRNA was well exported (Figure 2F-H). Note that versions of *ftz-Δi* lacking the 5'SS motif are not normally detectable in nuclear speckles under these conditions (Lee et al. 2015, 2022). Upon closer inspection, we noticed that at steady state *ftz-Δi-5'SS* also accumulates in other nuclear puncta that lack SC35. We do not know the nature of these structures although they may be related to YTHDC1-positive foci which were previously shown to partially overlap nuclear speckles and sequester m6A-rich mRNAs (Cheng et al. 2021), or "pA+ RNA foci" which accumulate both poly(A) RNAs, MTR4 and ZFC3H1 when the nuclear exosome is inhibited by RRP40-depletion (Silla et al. 2018). Our results may indicate that m6A may help transfer mRNAs from nuclear speckles to these other nuclear foci.

m6A methyltransferase METTL3 is required for the nuclear retention of misprocessed mRNAs

To further test whether m6A modifications were required for the nuclear retention of mRNAs with 5'SS motifs, we inhibited METTL3 by treating U2OS cells with the small molecule STM2457, which sterically blocks the S-adenosylmethionine-binding site of METTL3, thus inhibiting its RNA methylation activity (Yankova et al. 2021). Human U2OS cells expressing our *ftz* reporter (+/- the 5'SS motif) were treated with 100 μM STM2457 or DMSO as a control for 18 hours. We found that *ftz-Δi-5'SS* mRNA was no longer nuclear retained in STM2457-treated cells, when compared to DMSO-treated cells (Figure 3A-B). STM2457-treatment had no effect on the nuclear export of *ftz-Δi* mRNA. To further confirm this result, we depleted METTL3 using lentiviral-delivered shRNAs (Figure 3C) and expressed our various *ftz* reporters. Note that we use a combination of four shRNAs (with one targeted to exon 4 and one to exon 5 of *METTL3*) to prevent the expression of not only the main isoform, but other potential alternatively spliced versions (Poh et al. 2022). Indeed, we observe the disappearance of multiple bands after shRNA-treatment. In METTL3 depleted cells, we found that the 5'SS motif containing *ftz* reporter RNA was more cytoplasmic than in cells treated with control shRNA (Figure 3D-E).

In aggregate, these results demonstrate that the m6A modification is required for the nuclear retention of mRNAs containing intact 5'SS motifs.

YTHDC1 and YTHDC2 are required for the nuclear retention of 5'SS motif containing reporter mRNAs

To test whether YTHDC1 and YTHDC2 are required for the nuclear retention of mRNAs with intact 5'SS motifs in U2OS cells, we co-depleted these two proteins (Figure 4A) using two independent lentivirus-delivered shRNAs for each gene. In parallel, we depleted ZFC3H1, which

is required for the retention of mRNAs with intact 5'SS motifs (Lee et al. 2022), and ALKBH5, an m6A demethylase (results described in the next section) (Figure 4A).

We observed that in YTHDC1/2-co-depleted cells, *ftz-Δi-5'SS* mRNA was no longer efficiently retained in the nucleus when compared to control shRNA-treated cells (Figure 4B-C). The degree to which nuclear retention was inhibited in these cells was similar to ZFC3H1-depleted cells (Figure 4B-C). Both YTHDC1/2-co-depletion and ZFC3H1-depletion had no effect on the nuclear export of our reporter mRNAs that lacked either the 5'SS motif (*ftz-Δi*) or m6A modification motifs (*no-m6A-ftz-Δi-5'SS*).

Next, to validate our results with more natural IPA-generating genes, we monitored IPAs generated from two mini genes, *PCF11-IPA* and *CCDC71-IPA* (Figure 4D-I), that we had previously characterized (Lee et al. 2022). *PCF11-IPA* contains the first two exons and a truncated form of the first intron of the human *PCF11* gene (Figure 4D), while the *CCDC71-IPA* mini gene contains the first exon and intron of the human *CCDC17* gene (Figure 4G). These IPAs can then be specifically monitored by FISH using fluorescent probes that hybridize to the intronic region, just upstream of the 3'cleavage/polyadenylation site (Figure 4D, G). Both reporters are based on endogenous IPA transcripts and we previously found that they require both ZFC3H1 and U1-70K for their efficient nuclear retention (Lee et al. 2022). In agreement with our previous results, the two reporters were more cytoplasmic in cells co-depleted of YTHDC1 and YTHDC2 when compared to cells treated with control shRNA (Figure 4D-I).

Collectively, these results suggest that YTHDC1 and YTHDC2 are required for the efficient nuclear retention of mRNAs with intact 5'SS motifs. Moreover, as the absence of either feature (m6A sites and the 5'SS motif) leads to a complete loss of nuclear retention of our reporter

(Figure 2), and that YTHDC1, YTHDC2, ZFC3H1 and U1-70K interact (Figure 1), our results indicate that 5'SS motif recognition and m6A modification/recognition systems work together to nuclear retain and likely degrade RNAs.

Depletion of the m6A demethylase ALKBH5 inhibits nuclear retention of mRNAs with intact 5'SS motifs

If m6A was required to promote the nuclear retention of mRNAs with intact 5'SS motifs, we reasoned that depletion of enzymes that remove the m6A modification should enhance the nuclear retention of these transcripts. To test this, we depleted ALKBH5 in U2OS cells using lentiviral delivered shRNAs (Figure 4A). Note that due to the nature of our surprising results (see below) we used two different shRNAs to ensure that our findings were not due to off target effects.

Unexpectedly, we found that depletion of ALKBH5 inhibited the nuclear retention of *ftz-Δi-5'SS* mRNA (Figure 4B-C), *PCF11-IPA* (Figure 4D-F) and to a lesser extent *CCDC71-IPA* (Figure 4G-I). Depletion of ALKBH5 had no effect on the nuclear export of our reporter mRNAs that lacked either the 5'SS motif (*ftz-Δi*) or m6A modification motifs (*no-m6A-ftz-Δi-5'SS*) (Figure 4B-C). Consistent with previous reports (Zheng et al. 2013), we found that ALKBH5 was present in the nuclear fraction, although it was also present in the cytoplasm (Figure 4J). Thus, it is possible that ALKBH5 directly affects RNAs in the nucleus and impacts their retention or export.

From these results, we concluded that ALKBH5 was required for the efficient nuclear retention of most mRNAs that contained intact 5'SS motifs. We believe that this is likely due to either some indirect effect on overall m6A metabolism, or on the integrity of nuclear speckles (see discussion).

m6A methylation marks accumulate near the 5'SS motif and polyadenylation site in IPA transcripts

As the m6A machinery is required for the nuclear retention of 5'SS motif containing RNAs, which includes IPA transcripts, we next asked whether m6A methylation marks accumulate within natural IPA transcripts. To determine the genome wide distribution of m6A marks, we performed CLIP-seq using m6A specific antibody from total RNA isolated from HEK293 cells. The precise m6A site is inferred by identifying m6A antibody crosslink induced truncation sites, due to the fact that reverse transcriptase does not efficiently transcribe across crosslinked regions. We subsequently compared the distribution of these m6A methylation marks with all known intronic regions that have been previously shown to generate IPA transcripts. When the density of m6A modifications was averaged along the length of the intronic portion of IPAs, we found that these m6A marks were enriched near the start of the IPA (i.e., near the 5'SS motif) and near the 3'cleavage/polyadenylation site, when compared to the density of m6A averaged along all exons (Figure 5A). It should be noted that the level of the typical IPA transcript in a typical human cell is very low compared to the level of most exons. When we looked more closely at two example genes that generate IPA transcripts, *PCF11* and *CSNK1E*, we found that m6A-CLIP reads map throughout the intronic region that generates an IPA transcript (Figure 5B-C). Note that the level of both of these IPAs increases in ZFC3H1-depleted U2OS cells (Figure 5B-C).

Discussion

Here we show that m6A modifications and m6A binding proteins, in association with ZFC3H1 and U1-70K, are required for the nuclear retention of 5'SS motif containing RNAs. Moreover, we find that the m6A-binding proteins YTHDC1 and YTHDC2 associate with ZFC3H1 and U1-70K. It is thus likely that these factors form a complex that targets these misprocessed mRNAs for nuclear retention and possibly degradation by the nuclear exosome, which is known to receive substrate RNAs from the PAXT complex. These findings suggest that the m6A RNA methylation acts as an additional quality control layer by accumulating on misprocessed RNAs and promoting their nuclear retention and decay (Figure 6).

Although many reports have implicated m6A in promoting mRNA export and translation, more recent publications have found that m6A acts as a repressive mark both in terms of nuclear export (Smalec et al. 2022), RNA stability (Liu et al. 2020) and even feedback to silence chromatin regions that produce transposable element-derived RNA (Chen et al. 2021; Liu et al. 2021). Curiously, one of the reports that linked YTHDC1 to mRNA nuclear export also observed that upon the co-depletion of METTL3 and METTL14 there was a large increase in the cytoplasmic accumulation of mRNAs that are normally m6A modified, suggesting that m6A represses nuclear export (Roundtree et al. 2017). Other studies have found that when m6A modified mRNAs are in the cytoplasm, they are targeted for decay by UPF1 and the CCR4-NOT deadenylase complex, and this may represent a fail-safe mechanism to ensure the silencing of any m6A-rich mRNA that leaks into the cytoplasm (Wang et al. 2014; Du et al. 2016; Boo et al. 2022).

Recent work has demonstrated that m6A modifications are excluded from regions surrounding exon-exon splice site junctions by the exon-junction complex (EJC) (Yang et al. 2022; Uzonyi et al. 2023; He et al. 2023). It is unclear whether the EJC sterically inhibits the methylase

complex from modifying RNA regions surrounding exon junctions, or whether it promotes m6A removal by recruiting demethylases such as ALKBH5, which has been reported to associate with several components of the EJC (Covelo-Molares et al. 2021). Other methylases, such as METTL16, have also been reported to add m6A to retained introns, long non-coding RNAs (lncRNAs), and other non-coding RNAs (Warda et al. 2017), and this may also promote nuclear retention and decay. Our new results would indicate that m6A marks may be enhanced near intact 5'SS motifs and cryptic polyadenylation sites that are present in misprocessed transcripts. It has been recently observed that Nab2, an mRNA nuclear export factor that binds to the 3' end of mRNAs, also inhibits m6A deposition (Jalloh et al. 2023). Thus, it is possible that the enhancement or depletion of m6A at sites near the 3' end of an mRNA may play a critical role in determining whether it is exported or retained.

Based on these observations, we propose a model for how m6A contributes to quality control of mRNA processing (Figure 6). During biogenesis, pre-mRNAs are spliced allowing for the deposition of the EJC at exon-exon boundaries. This generates a zone of m6A exclusion near the splice site junctions, presumably by the association of the EJC with the ALKBH5 demethylase and/or by shielding RNA near the exon-exon junction from the methylase complex comprised of METTL3 and associated proteins. As a result, properly processed mRNAs are largely devoid of m6A methylation except in the 3' terminal exon and/or in long exons. In contrast, IPA transcripts, which form as a failure of splicing and do not recruit the EJC, accumulate a surplus of m6A modifications. These transcripts are thus recognized by both the U1 snRNP and YTHDC1/YTHDC2 which likely collaborate to recruit ZFC3H1, and likely other components of the PAXT complex to the transcript. This may be aided by PABPN1, which recognizes the poly(A)-tail, and the cap binding complex (CBP20 and CBP80), which binds to the PAXT complex through

the adaptor ARS2 (Meola et al. 2016). ZFC3H1 then targets these mRNAs for nuclear retention and decay.

One unresolved question is why the depletion of ALKBH5 promoted the nuclear export of IPA transcripts. One possible explanation is that ALKBH5-depletion disrupted nuclear speckles, as previously reported (Zheng et al. 2013), and nuclear speckles are required for the retention of reporter mRNAs with intact 5'SS motifs (Lee et al. 2022). When we stain U2OS cells depleted of ALKBH5 for the nuclear speckle marker SC35, we do not see any obvious changes to the nuclear speckles (data not shown). Nevertheless, it is possible that ALKBH5-depletion alters some property of nuclear speckles that is not obvious by gross inspection of immunofluorescent images against SC35. It is also possible that the depletion of ALKBH5 disrupts some aspect of the m6A metabolism. These indirect effects may also enhance general nuclear export, thus explaining previous reports linking m6A to nuclear export and not nuclear retention (Zheng et al. 2013).

Although components of the m6A machinery localize to nuclear speckles, there are some indications that m6A and the PAXT complex can also target mRNAs to different nuclear structures. In some human cells YTHDC1 targets certain m6A-modified mRNAs to nuclear foci, although these do not exactly correspond to nuclear speckles, and shields these mRNAs from the nuclear surveillance pathway (Cheng et al. 2021). When the exosome is inhibited in certain human cells, some ncRNAs and mRNAs that are targeted for destruction by PAXT also accumulate in nuclear foci that do not correspond to nuclear speckles, but contain ZFC3H1, MTR4 and other nuclear exosome components (Silla et al. 2018; Wang et al. 2021). Similar to YTHDC1, ZFC3H1 has many intrinsically disordered regions which can phase separate *in vitro*, and when overexpressed these ZFC3H1-enriched nuclear condensates only partially overlap with nuclear speckles (Wang et al. 2021). Strikingly, we have observed that mRNAs with intact 5'SS motifs are strongly enriched in

nuclear speckles soon after their synthesis (Lee et al. 2015, 2022 and Figure 2D). Consolidating our new results with our previous findings, it appears that mRNAs containing intact 5'SS motifs require nuclear speckles, perhaps to transit through, but may ultimately be retained in part in another nuclear structure in an m6A-dependent manner. It is also possible that at steady state these mRNAs partially partition to these various structures, but that they are not strictly retained in these locales. In agreement with this later view, RNAs that contain 5'SS motifs have quite high levels in the nucleoplasm that are not targeted to nuclear foci, yet this non-foci RNA does not appear to be exported to the cytoplasm.

Finally, our results strongly indicate that links between the m6A recognition proteins (i.e. YTH domain containing proteins) and the PAXT complex are evolutionarily conserved. In both humans and *S. pombe*, YTH domain containing proteins appear to be involved in suppressing transposable element-derived RNAs, suggesting additional conserved features. In *S. pombe*, both the MTREC complex and Mmi1 act together to degrade meiotic mRNAs that are inappropriately expressed in interphase cells. MTREC and Mmi1 are bridged by Erh1, which has a human homolog, ERH, that has been recently shown to regulate the stability of transposable element-derived RNAs and meiotic mRNAs (McCarthy et al. 2021). Thus, it is likely that many aspects of the MTREC-Mmi1 pathway in *S. pombe* are conserved in humans, and our latest results further confirm this idea. Future experiments need to be performed to determine whether other aspects of MTREC and Mmi1 function, including their regulation by TOR signalling and their ability to stimulate heterochromatin formation (Vo et al. 2019; Wei et al. 2021), are conserved in human cells.

Material and Methods

Plasmids constructs and antibodies

All plasmids for reporter constructs in pcDNA3.0, pcDNA3.1 (V5-His) or pcDNA5 are as previously described (Akef et al. 2013; Lee et al. 2015, 2020, 2022; Palazzo et al. 2007). All *no-m6A-ftz* reporters were synthesized and inserted in pUC57 plasmids (Genscript), subcloned using HindIII and SmaI sites and inserted into pcDNA3.0 or pcDNA3.1 (V5-His) respectively. The FLAG-HA-tagged YTHDC1 plasmid was purchased from Addgene (plasmid # 85167).

Antibodies used in this study include rabbit polyclonals against FLAG (Sigma, F7425), METTL3 (ABclonal, A8370), YTHDC1 (Abcam, ab122340), YTHDC2 (Abcam, ab176846), ALKBH5 (Atlas Antibodies, HPA007196), ZFC3H1 (Bethyl laboratories, A301-457A), U1-70K (Abcam, ab83306), and ALY (Zhou et al. 2000), and mouse monoclonals against SC35 (Sigma, Clone 35), FG-nucleoporins (Sigma, mAb414) and α-tubulin (Sigma, DM1A). Immunofluorescence was performed with Alexa647-conjugated secondaries (ThermoFisher) and HRP-conjugated secondaries (Cell Signaling). All antibodies were diluted 1:1000 to 1:2000 for western blotting.

Cell culture, DNA transfection, cell fractionation, and METTL3 inhibition by STM2457

U2OS and HEK293T cells were grown in DMEM media (Wisent) supplemented with 10% fetal bovine serum (FBS) (Wisent) and 5% penicillin/streptomycin (Wisent). DNA transfection experiments were performed as previously described (Akef et al. 2013; Lee et al. 2015, 2020, 2022; Palazzo et al. 2007). U2OS and HEK cells were transfected with the appropriate amount of

DNA plasmid according to the manufacturer's protocol using GenJet U2OS or Lipo293T DNA *in vitro* transfection reagent (SignaGen Laboratories) for 18 to 24 hrs.

Cell fractionation was performed as previously described (Lee et al. 2020). Equivalent amounts of nuclear and cytoplasmic lysates were analysed.

For METTL3 inhibition by STM2457, U2OS cells were transfected with the appropriate plasmids as described above. 6h post-transfection, cells were treated with 100 μM STM2457 (Sigma-Aldrich) or in DMSO for 18 hours. Cells were fixed and fluorescent in situ hybridization was performed as described below.

Fluorescent in situ hybridization (FISH) staining, immunostaining and analysis of nuclear speckle targeting

Fluorescent in situ hybridization and immunostaining were performed as previously described (Gueroussov et al. 2010; Lee et al. 2015, 2020, 2022).

Analysis of nuclear speckle targeting was performed as previously described (Akef et al. 2013). Each analysed region of interest consists of a rectangular region drawn to cover a single SC35-positive speckle and its surroundings (1–4 μm^2). Note that individual nuclear speckles were categorized using Pearson correlation coefficient intervals. For microinjected plasmid experiments, intervals of 0.1, from strongest (Pearson correlation of 1 to 0.9) to weakest (Pearson correlation of 0.6 to 0.5) were used. Any Pearson correlation coefficient < 0.5 was scored as "not localized". For transfected plasmid experiments, intervals of 0.15 were used with any Pearson correlation coefficient < 0.5 scored as "not localized".

Lentiviral delivered shRNA protein depletion

The lentiviral delivered shRNA protein depletion was performed as previously described (Akef et al. 2013; Lee et al. 2015, 2020, 2022). HEK293T were plated at 50% confluency on 60 mm dishes and transiently transfected with the gene specific shRNA pLKO.1 plasmid (Sigma), packaging plasmid (Δ8.9) and envelope (VSVG) vectors using Lipo293T DNA *in vitro* transfection reagent (SignaGen Laboratories) according to the manufacture's protocol. Viruses were harvested from the media 48 h post-transfection and added to U2OS cells pre-treated with 8 μg/ml hexadimethrine bromide. Cells were selected with 2 μg/ml puromycin media for at least 4 to 6 days. Western blotting was used to determine the efficiency of YTHDC1/YTHDC2, METTL3, ALKBH5 and ZFC3H1 depletion. The shRNAs constructs (Sigma) used in this study are as follows: ZFC3H1-2 "TRCN0000432333" 5'-CCGGGACTGA TGACATCGCT AATTTCTCGA GAAATTAGCG ATGTCATCAG TCTTTTTTG-3', YTHDC1-1 "TRCN0000243987" 5'-CCGGTGGATT TGCAGGCGTG AATTACTCGA GTAATTCACG CCTGCAAATC CATTTTTG -3', YTHDC1-2 "TRCN0000243988" 5'-CCGGCACCAG AGACCAGGGT ATTTACTCGA GTAAATACCC TGGTCTCTGG TGTTTTTG -3', YTHDC2-1 "TRCN0000157638" 5'-CCGGCGGAAG CTAAATCGAG CCTTTCTCGA GAAAGGCTCG ATTTAGCTTC CGTTTTTTG-3', YTHDC2-2 "TRCN0000232759" 5'-CCGGCAGAAG TGGCATAGCT TATTTCTCGA GAAATAAGCT ATGCCACTTC TGTTTTTG -3', ALKBH5-1 "TRCN0000064783" 5'-CCGGG AAAGG CTGTTGGCAT CAATACTCGA GTATTGATGC CAACAGCCTT TCTTTTTG-3', ALKBH5-2 "TRCN0000064787" 5'-CCGGCCTCAG GAAGACAAGA TTAGACTCGA GTCTAATCTT GTCTTCCTGA GGTTTTTG-3', METTL3-1 "TRCN0000034714" 5'-CCGGGCCTTA ACATTGCCCA CTGATCTCGA GATCAGTGGG CAATGTTAAG GCTTTTTG-3', METTL3-2 "TRCN0000034717" 5'- CCGGGCCAAG

GAACAATCCA TTGTTCTCGA GAACAATGGA TTGTTCCTTG GCTTTTTG-3', METTL3-3 "TRCN0000289743" 5'-CCGGGCAAGT ATGTTCACTA TGAAACTCGA GTTTCATAGT GAACATACTT GCTTTTTG-3', METTL3-4 "TRCN0000289812" 5'-CCGGCGTCAG TATCTTGGGC AAGTTCTCGA GAACTTGCCC AAGATACTGA CGTTTTTG-3'.

FLAG co-immunoprecipitation

FLAG co-immunoprecipitation was performed as previously described (Lee et al. 2022), except with these modifications. 1X 150 mm dish of HEK293 cells were transfected with either FLAG-HA-YTHDC1 or FLAG-ZFC3H1 (1-1233) using Lipo293T DNA *in vitro* transfection reagent (SignaGen Laboratories). 18 to 24 hours post transfection the cell pellets were trypsinized, collected and washed with 3 times with in ice-cold 1X PBS and flash frozen in liquid nitrogen. In parallel, another 150 mm dish of untransfected HEK293 cells of similar confluency was collected. The pellets were lysed in 2 ml lysis buffer (20 mM Tris-HCl, pH 8, 137 mM NaCl, 1% NP-40, 2 mM EDTA and *cOmplete* mini-protease inhibitor (Roche)) for 10 min rocking on a nutator at 4 °C. To ensure that the nuclear proteins were released from chromatin, the lysed sample was passed through a 25¾″ needle 5 times to shear the chromatin before incubation. The lysate was cleared by spinning at 16,100*g* for 10 minutes. ~950 µl of the lysate was added to ~50 to 60 µl FLAG M2 beads (Sigma-Aldrich, A2220), previously preincubated overnight with 5% BSA and 667 µg/ml Ultra-Pure salmon sperm DNA (Invitrogen), and incubated for 3 h at 4 °C. The remaining ~50 µl of the lysate was reserved as "INPUT", and 5X sample buffer was added and the sample was boiled at 95°C for 5 min. Following incubation, the FLAG M2 beads was washed 2 to 5 times with 300 mM wash buffer (20 mM Tris-HCl, pH 8, 300 mM NaCl, 0.05% NP-40, 2 mM EDTA and *cOmplete* mini-protease inhibitor (Roche)), 1 time with 137 mM wash buffer (same as for 300 mM

wash buffer, except with 137 mM NaCl) and transferred to a new Eppendorf tube. Subsequently, for RNase digested samples, ~400µl of 1:1000 RNase A/T1 (Thermo Scientific, EN055) diluted in 137 mM wash was added to the FLAG M2 beads and incubated for 20 min at 4°C. Samples that were not RNase digested were treated in the same manner, except the RNase A/T1 was omitted in the incubation mixture. The samples were washed 2 times with 137 mM wash buffer, transferred to a new Eppendorf tube and 50 to 100 µl 2.5X sample buffer was added to sample and boiled a 95°C for 5 min. Samples were separated on an SDS-PAGE gel and transferred onto a blot for immunoblotting.

m6A-miCLIP-seq

miCLIP-seq was performed as previously described (Linder et al. 2015), with modifications as detailed below. Briefly, cells were grown in independent batches to represent biological replicates. We extracted total RNA from HEK293 cells using TRIzol according to manufacturer's instructions. After RNA was treated with DNase I, 12 µg of total RNA was used for miCLIP-seq. 2 µl of RNA Fragmentation Reagents (Invitrogen AM8740) was added to the RNA suspended in 20 µl of sterile water. The mixture was incubated in a heat block at 75°C for exactly 12 minutes. Reaction was stopped by adding 2 µl of stop solution (Invitrogen AM8740). The fragmented RNA was incubated with 10 µg of m6A antibody (MBL RN131P) for 2 hours at 4°C. RNA-antibody complexes were UV crosslinked twice with 0.15 J/cm^2 at 254 nm in a Stratalinker 1800. 100µl of Protein G Dynabeads were added, and the samples were rotated for 2 hours at 4°C. Samples were washed three times using iCLIP high salt buffer with 5 min rotation in the cold room for each wash. RNA dephosphorylation was performed using FastAP and T4 polynucleotide kinase. Pre-adenylated L3 adaptors were ligated to the 3'-ends of RNAs using the

enhanced CLIP ligation method, as detailed previously (Nabeel-Shah and Greenblatt 2023). RNA was 5'-end-labeled with ^{32}P using T4 polynucleotide kinase (New England Biolabs catalogue number M0201L). Samples were separated using 4–12% BisTris-PAGE and transferred to a nitrocellulose membrane (Protran). RNA was recovered from the membrane by digesting proteins with proteinase K (Thermo Fisher catalogue number 25530049). Recovered RNA was reverse transcribed into cDNA using barcoded iCLIP primers. The cDNA was size-selected (low: 70 to 85 nt, middle: 85 to 110 nt, and high: 110 to 180 nt) using 6% TBE-Urea gels. cDNA was circularized using CircLigase™ II ssDNA ligase to add the adaptor to the 5'-end. We added betain at a final concentration of 1 M in the reaction and mixture was incubated for 2 hours at 60°C, as detailed previously (Nabeel-Shah and Greenblatt 2023). Circularized cDNA was digested at the internal BamHI site for linearization. Linearized cDNA was PCR amplified using Phusion High-Fidelity PCR Master Mix (NEB, M0531S).

The final PCR libraries were agarose gel purified on purification columns (QIAGEN). The eluted DNA was mixed at a ratio of 1:5:5 from the low, middle, and high fractions and submitted for sequencing on an Illumina NextSeq 500 platform to obtain single-end 51 nucleotide reads with 40 million read depth per sample. miCLIP-seq data is deposited at Gene Expression Omnibus (GEO, https://www.ncbi.nlm.nih.gov/geo/) with the accession code GSE230846 for the series, which contains several other datasets submitted as a part of Nabeel-Shah et al. (under review).

miCLIP-seq analysis

miCLIP-seq analyses were performed as detailed in our previous reports for iCLIP-seq (Song et al. 2022). Briefly, 51-nt miCLIP-seq raw reads that consist of 3 random positions, a 4-nt multiplexing barcode, and another 2 random positions, followed by the cDNA sequence were de-

duplicated based on the first 45 nt, and random positions, barcodes, and any 3′-bases matching Illumina adaptors were removed. Reads shorter than 25 nt were discarded, and the remaining reads were trimmed to 35nt using Trimmomatic (Bolger et al. 2014). Reads were mapped to the human genome/transcriptome (Ensembl annotation hg19) using Tophat (Trapnell et al. 2009) with default settings where reads with a mapping quality < 3 were removed from further analysis, which also removes multi-mapping reads.

Crosslinked induced truncations (CITS)

CLIP Tool Kit (CTK) was used to identify RNA-binding sites at single-nucleotide resolution (Shah et al. 2017). As miCLIP-seq aims to capture the crosslink-induced truncation sites (CITS) during cDNA preparation, we therefore called CITS, rather than CIMS (crosslink-induced mutations), on individual replicates. CITS with FDR ≤ 0.01 were considered as significant. CITS from 2 replicates were merged at a maximum gap of 1 bp. Each peak was then extended 2 bp both upstream and downstream of the identified CITS. Subsequently, only those CITS with a DRACH motif were selected and the coordinates of the base 'A' in the motif were designated as m6A sites.

Bioinformatic analysis

A list of introns that do not overlap with exons on the opposite strand was compiled from Gencode v.19. Intronic reads from shZFC3H1 U2OS Seq data (Lee et al. 2022) were analysed using rtracklayer (Lawrence et al. 2009) to identify introns with enrichment in the first 20% over the last 20%. Next, Introns with more overall reads in shZFC3H1 compared to shControl conditions were selected. IPA 5' splice sites were inferred from the PolyA feature annotation file from Gencode. m6A reads from miCLIP analysis (5,688 m6A peaks for IPA transcripts, 379,190

m6A peaks for exons) were aligned to IPAs or exons using their genomic coordinates and normalised to the length of the IPA or exon. The distribution was plotted using the ggplot2 density geometry (Wickham 2009). All bioinformatical analyses were done using R Statistical Software v4.2.2 (R Core Team 2022).

Research Contribution

E.S.L., H.W.S., S.S.J.I., L.S.O. and Y.E.W, performed the experiments under the guidance of A.F.P.. R.J. performed the bioinformatics analysis of m6A distribution under the guidance of A.F.P.. S.N.S performed the m6A-miCLIP experiments and S. P. performed the bioinformatics analysis under the guidance of J.F.G.

E.S.L. and A.F.P. co-wrote the paper, with input from all other authors.

Funding

This work was supported by a grant to AFP from Natural Sciences and Engineering Research Council of Canada (FN 492860).

Conflict of Interest

The authors have declared that no conflict of interest exists.

Acknowledgements

We thank members of the Donnelly Centre RNA sequencing facility for performing the m6A-miCLIP RNA sequencing. We thank G. L. Burke and N. Ahmed, for assistance with the m6A-miCLIP library preparation, J. Gao for her helpful discussions for the bioinformatics analysis and W.S. Tse for his technical expertise for our computational needs. We thank N.S.K. for feedback on the manuscript. Finally, we thank members of the Palazzo lab for their helpful discussions and insights.

References

Abad X, Vera M, Jung SP, Oswald E, Romero I, Amin V, Fortes P, Gunderson SI. 2008. Requirements for gene silencing mediated by U1 snRNA binding to a target sequence. *Nucleic Acids Res* **36**: 2338–2352.

Akef A, Zhang H, Masuda S, Palazzo AF. 2013. Trafficking of mRNAs containing ALREX-promoting elements through nuclear speckles. *Nucleus* **4**: 326–340.

Apponi LH, Leung SW, Williams KR, Valentini SR, Corbett AH, Pavlath GK. 2010. Loss of nuclear poly(A)-binding protein 1 causes defects in myogenesis and mRNA biogenesis. *Hum Mol Genet* **19**: 1058–1065.

Bolger AM, Lohse M, Usadel B. 2014. Trimmomatic: a flexible trimmer for Illumina sequence data. *Bioinformatics* **30**: 2114–2120.

Boo SH, Ha H, Lee Y, Shin M-K, Lee S, Kim YK. 2022. UPF1 promotes rapid degradation of m6A-containing RNAs. *Cell Reports* **39**: 110861.

Chen C, Liu W, Guo J, Liu Y, Liu X, Liu J, Dou X, Le R, Huang Y, Li C, et al. 2021. Nuclear m6A reader YTHDC1 regulates the scaffold function of LINE1 RNA in mouse ESCs and early embryos. *Protein Cell* **12**: 455–474.

Chen H-M, Futcher B, Leatherwood J. 2011. The fission yeast RNA binding protein Mmi1 regulates meiotic genes by controlling intron specific splicing and polyadenylation coupled RNA turnover. *PLoS One* **6**: e26804.

Cheng Y, Xie W, Pickering BF, Chu KL, Savino AM, Yang X, Luo H, Nguyen DTT, Mo S, Barin E, et al. 2021. N6-Methyladenosine on mRNA facilitates a phase-separated nuclear body that suppresses myeloid leukemic differentiation. *Cancer Cell* **39**: 958-972.e8.

Covelo-Molares H, Obrdlik A, Poštulková I, Dohnálková M, Gregorová P, Ganji R, Potěšil D, Gawriyski L, Varjosalo M, Vaňáčová Š. 2021. The comprehensive interactomes of human adenosine RNA methyltransferases and demethylases reveal distinct functional and regulatory features. *Nucleic Acids Research* **49**: 10895–10910.

Dias AP, Dufu K, Lei H, Reed R. 2010. A role for TREX components in the release of spliced mRNA from nuclear speckle domains. *Nat Commun* **1**: 97.

Dominissini D, Moshitch-Moshkovitz S, Schwartz S, Salmon-Divon M, Ungar L, Osenberg S, Cesarkas K, Jacob-Hirsch J, Amariglio N, Kupiec M, et al. 2012. Topology of the human and mouse m6A RNA methylomes revealed by m6A-seq. *Nature* **485**: 201–206.

Du H, Zhao Y, He J, Zhang Y, Xi H, Liu M, Ma J, Wu L. 2016. YTHDF2 destabilizes m(6)A-containing RNA through direct recruitment of the CCR4-NOT deadenylase complex. *Nat Commun* **7**: 12626.

Fan J, Kuai B, Wu G, Wu X, Chi B, Wang L, Wang K, Shi Z, Zhang H, Chen S, et al. 2017. Exosome cofactor hMTR4 competes with export adaptor ALYREF to ensure balanced nuclear RNA pools for degradation and export. *EMBO J* **36**: 2870–2886.

Fortes P, Cuevas Y, Guan F, Liu P, Pentlicky S, Jung SP, Martínez-Chantar ML, Prieto J, Rowe D, Gunderson SI. 2003. Inhibiting expression of specific genes in mammalian cells with 5' end-mutated U1 small nuclear RNAs targeted to terminal exons of pre-mRNA. *Proc Natl Acad Sci USA* **100**: 8264–8269.

Garland W, Jensen TH. 2020. Nuclear sorting of RNA. *WIREs RNA* **11**: e1572.

Goraczniak R, Behlke MA, Gunderson SI. 2009. Gene silencing by synthetic U1 adaptors. *Nat Biotechnol* **27**: 257–263.

Gueroussov S, Tarnawsky SP, Cui XA, Mahadevan K, Palazzo AF. 2010. Analysis of mRNA Nuclear Export Kinetics in Mammalian Cells by Microinjection. *J Vis Exp* **46**: 2387.

He PC, Wei J, Dou X, Harada BT, Zhang Z, Ge R, Liu C, Zhang L-S, Yu X, Wang S, et al. 2023. Exon architecture controls mRNA m6A suppression and gene expression. *Science* **379**: 677–682.

Ishigami Y, Ohira T, Isokawa Y, Suzuki Y, Suzuki T. 2021. A single m6A modification in U6 snRNA diversifies exon sequence at the 5' splice site. *Nat Commun* **12**: 3244.

Jalloh B, Lancaster CL, Rounds JC, Brown BE, Leung SW, Banerjee A, Morton DJ, Bienkowski RS, Fasken MB, Kremsky IJ, et al. 2023. The Drosophila Nab2 RNA binding protein inhibits m6A methylation and male-specific splicing of Sex lethal transcript in female neuronal tissue eds. D.L. Black and K. VijayRaghavan. *eLife* **12**: e64904.

Jia G, Fu Y, Zhao X, Dai Q, Zheng G, Yang Y, Yi C, Lindahl T, Pan T, Yang Y-G, et al. 2011. N6-methyladenosine in nuclear RNA is a major substrate of the obesity-associated FTO. *Nat Chem Biol* **7**: 885–887.

Kaida D, Berg MG, Younis I, Kasim M, Singh LN, Wan L, Dreyfuss G. 2010. U1 snRNP protects pre-mRNAs from premature cleavage and polyadenylation. *Nature* **468**: 664–668.

Lawrence M, Gentleman R, Carey V. 2009. rtracklayer: an R package for interfacing with genome browsers. *Bioinformatics* **25**: 1841–1842.

Lee ES, Akef A, Mahadevan K, Palazzo AF. 2015. The consensus 5' splice site motif inhibits mRNA nuclear export. *PLoS One* **10**: e0122743.

Lee ES, Smith HW, Wolf EJ, Guvenek A, Wang YE, Emili A, Tian B, Palazzo AF. 2022. ZFC3H1 and U1-70K promote the nuclear retention of mRNAs with 5' splice site motifs within nuclear speckles. *RNA* **28**: 878–894.

Lee ES, Wolf EJ, Ihn SSJ, Smith HW, Emili A, Palazzo AF. 2020. TPR is required for the efficient nuclear export of mRNAs and lncRNAs from short and intron-poor genes. *Nucleic Acids Res* **48**: 11645–11663.

Legrain P, Rosbash M. 1989. Some cis- and trans-acting mutants for splicing target pre-mRNA to the cytoplasm. *Cell* **57**: 573–583.

Lesbirel S, Viphakone N, Parker M, Parker J, Heath C, Sudbery I, Wilson SA. 2018. The m6A-methylase complex recruits TREX and regulates mRNA export. *Sci Rep* **8**: 13827.

Lesbirel S, Wilson SA. 2019. The m6A-methylase complex and mRNA export. *Biochimica et Biophysica Acta (BBA) - Gene Regulatory Mechanisms* **1862**: 319–328.

Linder B, Grozhik AV, Olarerin-George AO, Meydan C, Mason CE, Jaffrey SR. 2015. Single-nucleotide-resolution mapping of m6A and m6Am throughout the transcriptome. *Nat Methods* **12**: 767–772.

Liu J, Dou X, Chen C, Chen C, Liu C, Xu MM, Zhao S, Shen B, Gao Y, Han D, et al. 2020. N6-methyladenosine of chromosome-associated regulatory RNA regulates chromatin state and transcription. *Science* **367**: 580–586.

Liu J, Gao M, He J, Wu K, Lin S, Jin L, Chen Y, Liu H, Shi J, Wang X, et al. 2021. The RNA m6A reader YTHDC1 silences retrotransposons and guards ES cell identity. *Nature* **591**: 322–326.

Liu J, Yue Y, Han D, Wang X, Fu Y, Zhang L, Jia G, Yu M, Lu Z, Deng X, et al. 2014. A METTL3-METTL14 complex mediates mammalian nuclear RNA N6-adenosine methylation. *Nat Chem Biol* **10**: 93–95.

McCarthy RL, Kaeding KE, Keller SH, Zhong Y, Xu L, Hsieh A, Hou Y, Donahue G, Becker JS, Alberto O, et al. 2021. Diverse heterochromatin-associated proteins repress distinct classes of genes and repetitive elements. *Nat Cell Biol* **23**: 905–914.

Meola N, Domanski M, Karadoulama E, Chen Y, Gentil C, Pultz D, Vitting-Seerup K, Lykke-Andersen S, Andersen JS, Sandelin A, et al. 2016. Identification of a Nuclear Exosome Decay Pathway for Processed Transcripts. *Mol Cell* **64**: 520–533.

Meyer KD, Saletore Y, Zumbo P, Elemento O, Mason CE, Jaffrey SR. 2012. Comprehensive analysis of mRNA methylation reveals enrichment in 3' UTRs and near stop codons. *Cell* **149**: 1635–1646.

Nabeel-Shah S, Greenblatt J. 2023. Revised iCLIP-seq Protocol for Profiling RNA–protein Interaction Sites at Individual Nucleotide Resolution in Living Cells. *BIO-PROTOCOL* **13**: e4688.

Nayler O, Hartmann AM, Stamm S. 2000. The ER Repeat Protein Yt521-B Localizes to a Novel Subnuclear Compartment. *J Cell Biol* **150**: 949–962.

Ogami K, Manley JL. 2017. Mtr4/ZFC3H1 protects polysomes through nuclear RNA surveillance. *Cell Cycle* **16**: 1999–2000.

Ogami K, Richard P, Chen Y, Hoque M, Li W, Moresco JJ, Yates JR, Tian B, Manley JL. 2017. An Mtr4/ZFC3H1 complex facilitates turnover of unstable nuclear RNAs to prevent their cytoplasmic transport and global translational repression. *Genes Dev* **31**: 1257–1271.

Palazzo AF, Lee ES. 2018. Sequence Determinants for Nuclear Retention and Cytoplasmic Export of mRNAs and lncRNAs. *Front Genet* **9**: 440.

Palazzo AF, Springer M, Shibata Y, Lee C-S, Dias AP, Rapoport TA. 2007. The signal sequence coding region promotes nuclear export of mRNA. *PLoS Biol* **5**: e322.

Poh HX, Mirza AH, Pickering BF, Jaffrey SR. 2022. Alternative splicing of METTL3 explains apparently METTL3-independent m6A modifications in mRNA. *PLOS Biology* **20**: e3001683.

R Core Team. 2022. R: A language and environment for statistical computing. https://www.R-project.org/.

Roundtree IA, Luo G-Z, Zhang Z, Wang X, Zhou T, Cui Y, Sha J, Huang X, Guerrero L, Xie P, et al. 2017. YTHDC1 mediates nuclear export of N6-methyladenosine methylated mRNAs. *Elife* **6**: e31311.

Shah A, Qian Y, Weyn-Vanhentenryck SM, Zhang C. 2017. CLIP Tool Kit (CTK): a flexible and robust pipeline to analyze CLIP sequencing data. *Bioinformatics* **33**: 566–567.

Shibuya T, Tange TØ, Sonenberg N, Moore MJ. 2004. eIF4AIII binds spliced mRNA in the exon junction complex and is essential for nonsense-mediated decay. *Nat Struct Mol Biol* **11**: 346–351.

Shichino Y, Otsubo Y, Kimori Y, Yamamoto M, Yamashita A. 2018. YTH-RNA-binding protein prevents deleterious expression of meiotic proteins by tethering their mRNAs to nuclear foci ed. T.H. Jensen. *eLife* **7**: e32155.

Shichino Y, Otsubo Y, Yamamoto M, Yamashita A. 2020. Meiotic gene silencing complex MTREC/NURS recruits the nuclear exosome to YTH-RNA-binding protein Mmi1. *PLOS Genetics* **16**: e1008598.

Silla T, Karadoulama E, Mąkosa D, Lubas M, Jensen TH. 2018. The RNA Exosome Adaptor ZFC3H1 Functionally Competes with Nuclear Export Activity to Retain Target Transcripts. *Cell Rep* **23**: 2199–2210.

Silla T, Schmid M, Dou Y, Garland W, Milek M, Imami K, Johnsen D, Polak P, Andersen JS, Selbach M, et al. 2020. The human ZC3H3 and RBM26/27 proteins are critical for PAXT-mediated nuclear RNA decay. *Nucleic Acids Res* **48**: 2518–2530.

Smalec BM, Ietswaart R, Choquet K, McShane E, West ER, Churchman LS. 2022. Genome-wide quantification of RNA flow across subcellular compartments reveals determinants of the mammalian transcript life cycle. 2022.08.21.504696. https://www.biorxiv.org/content/10.1101/2022.08.21.504696v1 (Accessed January 5, 2023).

Song J, Nabeel-Shah S, Pu S, Lee H, Braunschweig U, Ni Z, Ahmed N, Marcon E, Zhong G, Ray D, et al. 2022. Regulation of alternative polyadenylation by the C2H2-zinc-finger protein Sp1. *Mol Cell* **82**: 3135-3150.e9.

Spector DL, Fu XD, Maniatis T. 1991. Associations between distinct pre-mRNA splicing components and the cell nucleus. *EMBO J* **10**: 3467–3481.

Sugiyama T, Sugioka-Sugiyama R. 2011. Red1 promotes the elimination of meiosis-specific mRNAs in vegetatively growing fission yeast. *EMBO J* **30**: 1027–1039.

Sugiyama T, Thillainadesan G, Chalamcharla VR, Meng Z, Balachandran V, Dhakshnamoorthy J, Zhou M, Grewal SIS. 2016. Enhancer of Rudimentary Cooperates with Conserved RNA-Processing Factors to Promote Meiotic mRNA Decay and Facultative Heterochromatin Assembly. *Mol Cell* **61**: 747–759.

Tian B, Pan Z, Lee JY. 2007. Widespread mRNA polyadenylation events in introns indicate dynamic interplay between polyadenylation and splicing. *Genome Res* **17**: 156–165.

Trapnell C, Pachter L, Salzberg SL. 2009. TopHat: discovering splice junctions with RNA-Seq. *Bioinformatics* **25**: 1105–1111.

Ueda Y, Ooshio I, Fusamae Y, Kitae K, Kawaguchi M, Jingushi K, Hase H, Harada K, Hirata K, Tsujikawa K. 2017. AlkB homolog 3-mediated tRNA demethylation promotes protein synthesis in cancer cells. *Sci Rep* **7**: 42271.

Uzonyi A, Dierks D, Nir R, Kwon OS, Toth U, Barbosa I, Burel C, Brandis A, Rossmanith W, Le Hir H, et al. 2023. Exclusion of m6A from splice-site proximal regions by the exon junction complex dictates m6A topologies and mRNA stability. *Mol Cell* **83**: 237-251.e7.

Veitia RA. 2007. Exploring the Molecular Etiology of Dominant-Negative Mutations. *Plant Cell* **19**: 3843–3851.

Vo TV, Dhakshnamoorthy J, Larkin M, Zofall M, Thillainadesan G, Balachandran V, Holla S, Wheeler D, Grewal SIS. 2019. CPF Recruitment to Non-canonical Transcription Termination Sites Triggers Heterochromatin Assembly and Gene Silencing. *Cell Rep* **28**: 267-281.e5.

Wang C, Zhu Y, Bao H, Jiang Y, Xu C, Wu J, Shi Y. 2016. A novel RNA-binding mode of the YTH domain reveals the mechanism for recognition of determinant of selective removal by Mmi1. *Nucleic Acids Res* **44**: 969–982.

Wang K, Wang L, Wang J, Chen S, Shi M, Cheng H. 2018. Intronless mRNAs transit through nuclear speckles to gain export competence. *J Cell Biol* **217**: 3912–3929.

Wang X, Lu Z, Gomez A, Hon GC, Yue Y, Han D, Fu Y, Parisien M, Dai Q, Jia G, et al. 2014. m6A-dependent regulation of messenger RNA stability. *Nature* **505**: 117–120.

Wang Y, Fan J, Wang J, Zhu Y, Xu L, Tong D, Cheng H. 2021. ZFC3H1 prevents RNA trafficking into nuclear speckles through condensation. *Nucleic Acids Research* **49**: 10630–10643.

Warda AS, Kretschmer J, Hackert P, Lenz C, Urlaub H, Höbartner C, Sloan KE, Bohnsack MT. 2017. Human METTL16 is a N6-methyladenosine (m6A) methyltransferase that targets pre-mRNAs and various non-coding RNAs. *EMBO Rep* **18**: 2004–2014.

Wei Y, Lee NN, Pan L, Dhakshnamoorthy J, Sun L-L, Zofall M, Wheeler D, Grewal SIS. 2021. TOR targets an RNA processing network to regulate facultative heterochromatin, developmental gene expression and cell proliferation. *Nat Cell Biol* **23**: 243–256.

Wickham H. 2009. *Ggplot2: elegant graphics for data analysis*. Springer, New York.

Xu C, Wang X, Liu K, Roundtree IA, Tempel W, Li Y, Lu Z, He C, Min J. 2014. Structural basis for selective binding of m6A RNA by the YTHDC1 YTH domain. *Nat Chem Biol* **10**: 927–929.

Xu Y, Zhang W, Shen F, Yang X, Liu H, Dai S, Sun X, Huang J, Guo Q. 2021. YTH Domain Proteins: A Family of m6A Readers in Cancer Progression. *Frontiers in Oncology* **11**: 629560.

Yang X, Triboulet R, Liu Q, Sendinc E, Gregory RI. 2022. Exon junction complex shapes the m6A epitranscriptome. *Nat Commun* **13**: 7904.

Yankova E, Blackaby W, Albertella M, Rak J, De Braekeleer E, Tsagkogeorga G, Pilka ES, Aspris D, Leggate D, Hendrick AG, et al. 2021. Small-molecule inhibition of METTL3 as a strategy against myeloid leukaemia. *Nature* **593**: 597–601.

Zheng G, Dahl JA, Niu Y, Fedorcsak P, Huang C-M, Li CJ, Vågbø CB, Shi Y, Wang W-L, Song S-H, et al. 2013. ALKBH5 Is a Mammalian RNA Demethylase that Impacts RNA Metabolism and Mouse Fertility. *Mol Cell* **49**: 18–29.

Zhou Y, Zhu J, Schermann G, Ohle C, Bendrin K, Sugioka-Sugiyama R, Sugiyama T, Fischer T. 2015. The fission yeast MTREC complex targets CUTs and unspliced pre-mRNAs to the nuclear exosome. *Nat Commun* **6**: 1–11.

Zhou Z, Luo MJ, Straesser K, Katahira J, Hurt E, Reed R. 2000. The protein Aly links pre-messenger-RNA splicing to nuclear export in metazoans. *Nature* **407**: 401–405.

Figure Legends

Figure 1. m6A machinery forms a complex with nuclear surveillance factors

(A) The main components of the MTREC complex (outlined by a dotted line) and associated factors in *S. pombe* (left), and their human homologs, including the PAXT complex (outlined by a dotted line) and YTH proteins (right).

(B-C) HEK293 cells were either transfected with FLAG-tagged YTHDC1 or mock transfected. 18-24 hr cell lysates were collected and subjected to immunoprecipitation using FLAG M2 beads. Precipitates were then treated with either buffer or a combination of RNase A and RNase T1 and reisolated. Note that YTHDC2, ZFC3H1 and U1-70K were present in the precipitates in an RNase-independent manner. In contrast, eIF4AIII levels in the precipitates greatly decreased after RNase-treatment. ALKBH5 or ALY was not detectable in any of the immunoprecipitates.

(D-E) Similar to (B-C), except that cells were transfected with a FLAG-tagged fragment of ZFC3H1 (1-1233). In FLAG-ZFC3H1 expressing immunoprecipitates, YTHDC1, YTHDC2 and U1-70K were detected in an RNA independent manner. ALKBH5, METTL3, ALY and eIF4AIII were not detected in FLAG-tagged immunoprecipitates.

Figure 2. The m6A modification is required for nuclear retention of 5'SS motif containing mRNAs

(A) Schematic of the intronless fushi-tarazu (*ftz-Δi*) reporters used in this study, with and without the 5'SS motif in the 3'UTR. Note that the consensus 5'SS motif promotes nuclear retention. The

consensus DRACH motifs, the mutated forms that eliminate these motifs (AGGCT), and the mutated forms that enhance these motifs (AGACT) are indicated.

(B-C) U2OS cells were transfected with the various *ftz* reporters, +/- the 5'SS motif, +/- DRACH motifs. 18-24 h later the cells were fixed and the mRNA was visualized by FISH. The lack of DRACH motifs caused the cytoplasmic accumulation of *ftz-Δi-5'SS* mRNAs. Representative images are shown in (C), scale bar = 20 µm, and quantification is shown in (D). Each bar represents the average and standard error of at least three independent experiments, each experiment consisting of at least 30 to 60 cells. Student t-test was performed, *** $p < 0.001$.

(D-E) Plasmid DNA containing the *ftz-Δi-5'SS* or *no-m6A-ftz-Δi-5'SS* reporter genes was microinjected into U2OS nuclei. One hour post-injection, cells were fixed and stained for *ftz* mRNA by FISH and SC35 by immunofluorescence. (D) Each row represents a single field of view. The color overlay shows mRNA in red and SC35 in green in. Speckles containing mRNA are indicated by arrows (Scale bar = 10µm). (E) Microinjected cells were analysed for the distribution of mRNAs into nuclear speckles. Individual nuclear speckles (SC35 stained) were analysed for mRNA content by Pearson's Correlation Analysis. Each bar is the average and standard error of the mean of three experiments, each experiment consist of 100 nuclear speckles analysed from 10 cells.

(F-H) Plasmid DNA containing the *ftz-Δi-5'SS* or *no-m6A-ftz-Δi-5'SS* reporter genes was transfected into U2OS. 24 hours post-transfection, cells were fixed and stained for *ftz* mRNA by FISH and SC35 by immunofluorescence. (F) Images of *ftz* mRNA by FISH, scale bar = 10µm. Note that *ftz-Δi-5'SS* mRNA is mostly nuclear and *no-m6A-ftz-Δi-5'SS* is mostly cytoplasmic. The boxed areas in (F) are enlarged in (G), where each row represents a single field of view. The color

overlay shows mRNA in red and SC35 in green in. Speckles containing mRNA are indicated by arrows (Scale bar = 10μm). (H) Individual nuclear speckles (SC35 stained) were analysed for mRNA content by Pearson's Correlation Analysis. Each bar is the average and standard deviation of two experiments, each experiment consist of >100 nuclear speckles analysed from 10 cells.

Figure 3. The methyltransferase METTL3 is required for the nuclear retention of 5'SS motif containing mRNAs

(A-B) U2OS cells were transfected with the various *ftz* reporters, +/- the 5'SS motif. 6h post transfection, cells were treated with 100 μM STM2457 or DMSO. 18 hours later, the cells were fixed and the mRNA was visualized by FISH. Representative images are shown in (A), scale bar = 20 μm, and quantification shown in (B). Each bar represents the average and standard error of at least three independent experiments, each experiment consisting of at least 30 to 60 cells. Student t-test was performed, * $p < 0.05$.

(C) U2OS cells were treated with lentivirus containing four different shRNAs against METTL3 or scrambled control shRNA. Lysates were collected after 96 hrs, separated by SDS-PAGE, and immunoprobed for METTL3 or tubulin. Note that shRNA-treatment results in the depletion of multiple METTL3-positive bands, which may represent different spliced isoforms.

(D-E) Control- or METTL3-depleted cells were transfected with the intronless *ftz* reporter plasmid (+/- 5'SS). 18-24 hours later the cells were fixed and the mRNA was visualized by FISH. Depletion of METTL3 caused cytoplasmic accumulation of *ftz-Δi-5'SS*. METTL3 depletion leads to cytoplasmic accumulation of *ftz-Δi-5'SS*. Representative images are shown in (D), scale bar = 20 μm, and quantification is shown in (E). Each bar represents the average and standard error of three

independent experiments, each experiment consisting of at least 30 to 60 cells. Student t-test was performed, ** $p < 0.01$.

Figure 4. YTHDC1/YTHDC2 and ALKBH5 are required for the nuclear retention of 5'SS motif containing mRNAs

(A) U2OS cells were treated with different lentivirus shRNAs against YTHDC1, YTHDC2, ALKBH5, ZFC3H1 or scrambled control. Note that "ZFC3H1-2" denotes shRNA #2 against ZFC3H1 as described previously (Lee et al. 2022). Lysates were collected after 96 hrs, separated by SDS-PAGE and immunoprobed for YTHDC1, YTHDC2, ALKBH5, ZFC3H1, tubulin or mAb414, which recognizes FG-Nucleoporin proteins. To effectively deplete YTHDC1 and YTHDC2, cells were treated with lentivirus containing two shRNAs against YTHDC1 and another two against YTHDC2.

(B-C) Control- or YTHDC1/2-, ALKBH5-, ZFC3H1-depleted cells were transfected with the intronless *ftz* reporter plasmid (+/- 5'SS) and 5'SS motif containing reporter that lacks m6A methylation sites (*no-m6A-ftz-Δi-5'SS*). 18-24 hours later the cells were fixed and the mRNA was visualized by FISH. Depletion of YTHDC1/YTHDC2, ALKBH5 and ZFC3H1 caused cytoplasmic accumulation of *ftz-Δi-5'SS* and enhanced the cytoplasmic levels of *no-m6A-ftz-Δi-5'SS*. Representative images are shown in (B), scale bar = 20 µm, and quantification is shown in (C). Each bar represents the average and standard error of three independent experiments, each experiment consisting of at least 30 to 60 cells. Student t-test was performed, * $p < 0.05$, ** $p < 0.01$, *** $p < 0.001$.

(D) Schematic of *PCF11-IPA* RNA reporter. The position of the FISH probe used to visualize the IPA RNA is marked in gray and the position of the 3′ cleavage site in the intron is as indicated.

(E-F) Similar to (B-C), except that Control-, YTHDC1/YTHDC2- or ALKBH5-depleted cells were transfected with the *PCF11-IPA* RNA reporter.

(G) Schematic of *CCDC71-IPA* RNA reporter. The position of the FISH probe used to visualize the IPA RNA is marked in gray and the position of the 3′ cleavage site in the intron is as indicated.

(H-I) Similar to (B-C), except that Control-, YTHDC1/YTHDC2- or ALKBH5-depleted cells were transfected with the *CCDC71-IPA* RNA reporter.

(J) U2OS cell were fractionated into nuclear and cytoplasmic fractions which were separated by SDS-PAGE and immunoprobed for ALKBH5. To determine the purity of each fraction, tubulin, a cytoplasmic marker, and ALY, a nuclear marker were immunoprobed.

Figure 5. m6A methylation marks accumulate near the 5'SS motif and polyadenylation site in IPA transcripts

(A) Metanalysis of m6A density (as determined by m6A-miCLIP RNA-seq) along intronic portions of IPA transcripts from 5'SS motif to poly(A)-tail (dark blue) and all exons from the 5' to 3' ends (cyan). 5,688 m6A peaks were analyzed in 974 IPA transcripts, while 379,190 m6A peaks were analyzed in 1,296,308 exons. Note that m6A methylation marks are enriched near the 5'SS motif and poly(A) sites of IPA transcripts, and depleted from the 5' and 3' ends of exons.

(B-C) Two examples IPA transcripts that accumulate m6A density. Integrative Genomics Viewer (IGV) browser tracks are shown for miCLIP density for the *PCF11* IPA transcript in (B) and

CSNK1E IPA transcript in (C). Intronic cleavage/polyadenylation site is indicated by the red arrow. Total RNA sequencing levels in U2OS cells from previously published work (Lee et al. 2022) is shown. Note that the levels of IPA transcripts are upregulated following ZFC3H1 depletion (shZFC).

Figure 6. m6A acts as a layer of nuclear surveillance for 5'SS motif containing mRNAs

Model of how the m6A methylation mark is required for the nuclear surveillance of 5'SS motif containing mRNAs (see text for more details).

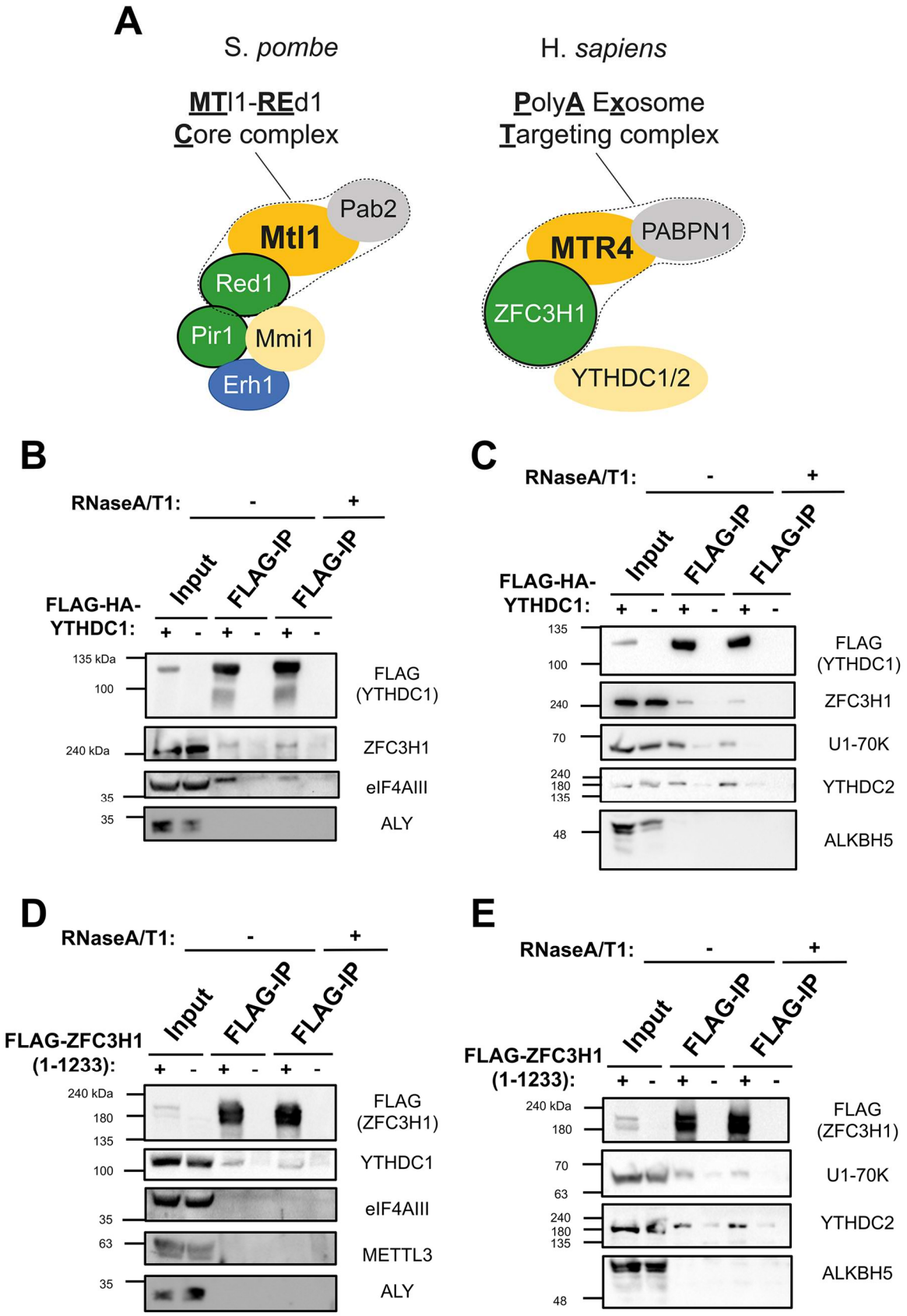
A
S. pombe
MTl1-REd1
Core complex
Pab2
Mtl1
Red1
Pir1
Mmi1
Erh1
H. sapiens
PolyA Exosome
Targeting complex
PABPN1
MTR4
ZFC3H1
YTHDC1/2
B
RNaseA/T1: - +
Input
FLAG-IP
FLAG-IP
FLAG-HA-YTHDC1: + - + - + -
135 kDa
100
FLAG (YTHDC1)
240 kDa
ZFC3H1
35
eIF4AIII
35
ALY
C
RNaseA/T1: - +
Input
FLAG-IP
FLAG-IP
FLAG-HA-YTHDC1: + - + - + -
135
100
FLAG (YTHDC1)
240
ZFC3H1
70
U1-70K
240
180
135
YTHDC2
48
ALKBH5
D
RNaseA/T1: - +
Input
FLAG-IP
FLAG-IP
FLAG-ZFC3H1 (1-1233): + - + - + -
240 kDa
180
135
FLAG (ZFC3H1)
100
YTHDC1
35
eIF4AIII
63
METTL3
35
ALY
E
RNaseA/T1: - +
Input
FLAG-IP
FLAG-IP
FLAG-ZFC3H1 (1-1233): + - + - + -
240 kDa
180
FLAG (ZFC3H1)
70
63
U1-70K
240
180
135
YTHDC2
ALKBH5
48

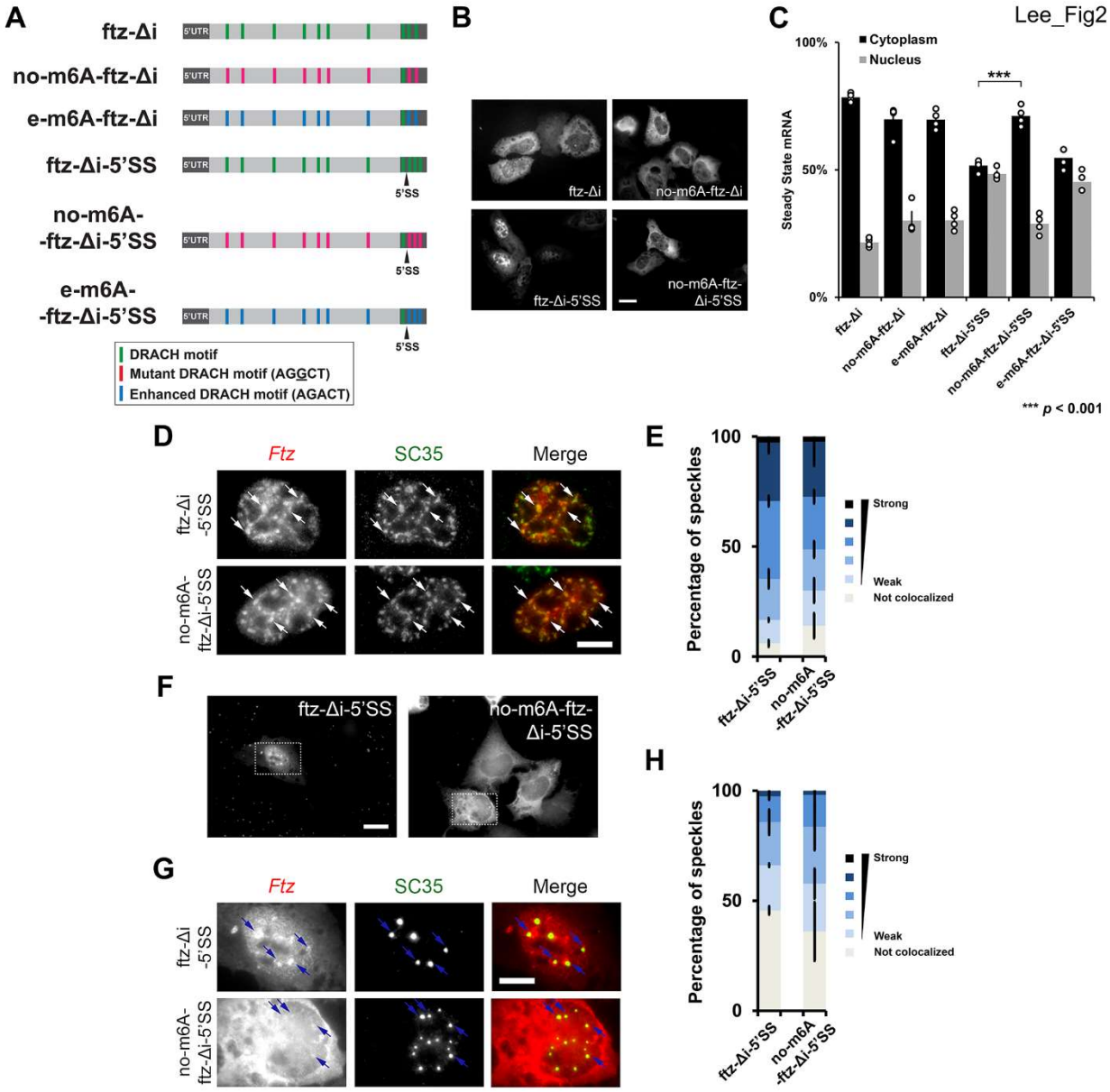
A
ftz-Δi
no-m6A-ftz-Δi
e-m6A-ftz-Δi
ftz-Δi-5'SS
no-m6A-ftz-Δi-5'SS
e-m6A-ftz-Δi-5'SS
5'UTR
5'SS
DRACH motif
Mutant DRACH motif (AGGCT)
Enhanced DRACH motif (AGACT)
B
ftz-Δi
no-m6A-ftz-Δi
ftz-Δi-5'SS
no-m6A-ftz-Δi-5'SS
C
Lee_Fig2
Cytoplasm
Nucleus
Steady State mRNA
100%
50%
0%
***
ftz-Δi
no-m6A-ftz-Δi
e-m6A-ftz-Δi
ftz-Δi-5'SS
no-m6A-ftz-Δi-5'SS
e-m6A-ftz-Δi-5'SS
*** p < 0.001
D
Ftz
SC35
Merge
ftz-Δi -5'SS
no-m6A-ftz-Δi-5'SS
E
Percentage of speckles
100
50
0
Strong
Weak
Not colocalized
ftz-Δi-5'SS
no-m6A -ftz-Δi-5'SS
F
ftz-Δi-5'SS
no-m6A-ftz-Δi-5'SS
G
Ftz
SC35
Merge
ftz-Δi -5'SS
no-m6A-ftz-Δi-5'SS
H
Percentage of speckles
100
50
0
Strong
Weak
Not colocalized
ftz-Δi-5'SS
no-m6A -ftz-Δi-5'SS

Lee_Fig3

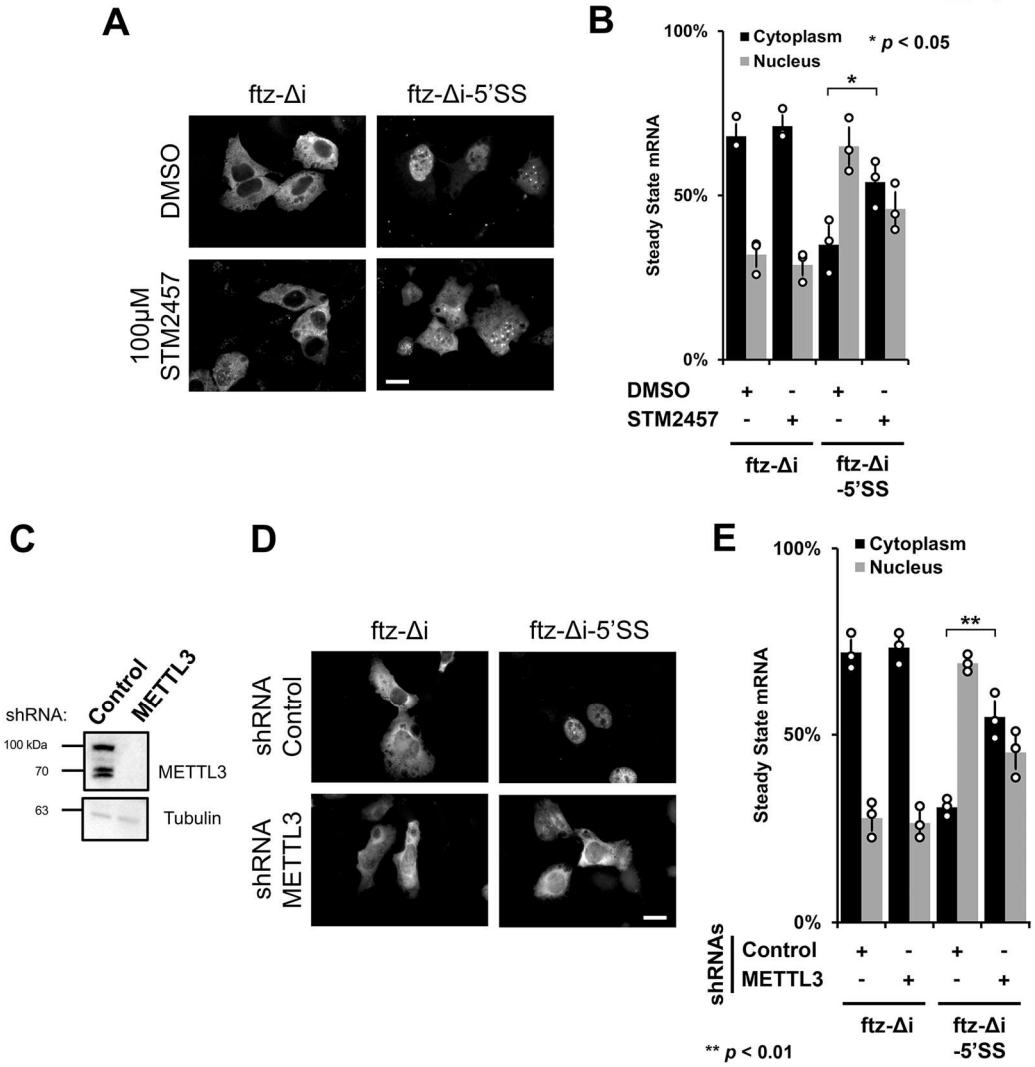
A
ftz-Δi
ftz-Δi-5'SS
DMSO
100μM STM2457
B
100%
50%
0%
Cytoplasm
Nucleus
* p < 0.05
*
Steady State mRNA
DMSO + - + -
STM2457 - + - +
ftz-Δi
ftz-Δi -5'SS
C
shRNA:
Control
METTL3
100 kDa
70
63
METTL3
Tubulin
D
ftz-Δi
ftz-Δi-5'SS
shRNA Control
shRNA METTL3
E
100%
50%
0%
Cytoplasm
Nucleus
**
Steady State mRNA
shRNAs
Control + - + -
METTL3 - + - +
ftz-Δi
ftz-Δi -5'SS
** p < 0.01

Lee_Fig4

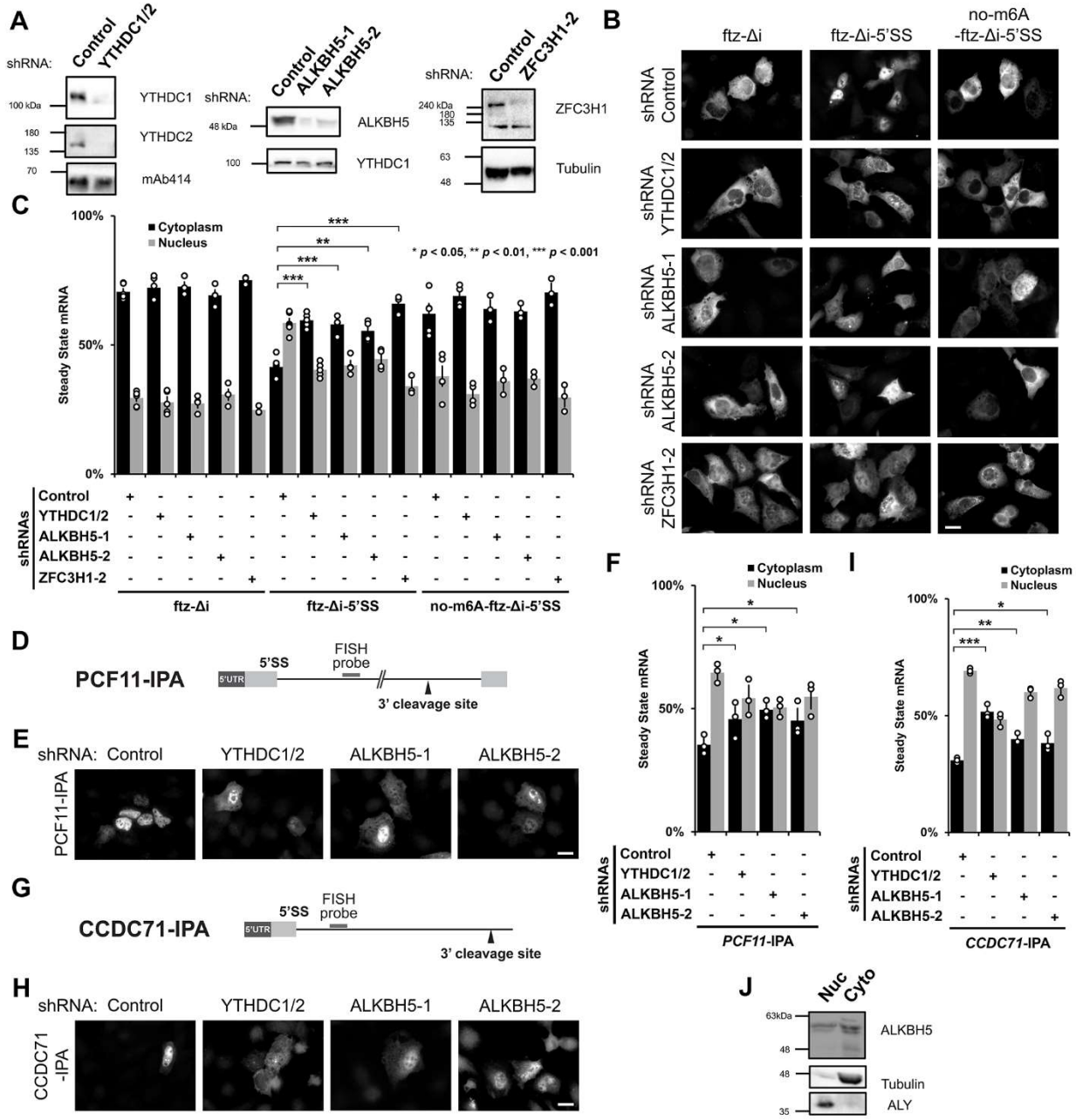
A
shRNA: Control YTHDC1/2
100 kDa
180
135
70
YTHDC1
YTHDC2
mAb414
shRNA: Control ALKBH5-1 ALKBH5-2
48 kDa
100
ALKBH5
YTHDC1
shRNA: Control ZFC3H1-2
240 kDa
180
135
63
48
ZFC3H1
Tubulin
B
ftz-Δi
ftz-Δi-5'SS
no-m6A -ftz-Δi-5'SS
shRNA Control
shRNA YTHDC1/2
shRNA ALKBH5-1
shRNA ALKBH5-2
shRNA ZFC3H1-2
C
Cytoplasm
Nucleus
* p < 0.05, ** p < 0.01, *** p < 0.001
Steady State mRNA
100%
50%
0%
shRNAs
Control
YTHDC1/2
ALKBH5-1
ALKBH5-2
ZFC3H1-2
ftz-Δi
ftz-Δi-5'SS
no-m6A-ftz-Δi-5'SS
D
PCF11-IPA
5'UTR
5'SS
FISH probe
3' cleavage site
E
shRNA: Control
YTHDC1/2
ALKBH5-1
ALKBH5-2
PCF11-IPA
G
CCDC71-IPA
5'UTR
5'SS
FISH probe
3' cleavage site
H
shRNA: Control
YTHDC1/2
ALKBH5-1
ALKBH5-2
CCDC71 -IPA
F
Cytoplasm
Nucleus
Steady State mRNA
100%
50%
0%
shRNAs
Control
YTHDC1/2
ALKBH5-1
ALKBH5-2
PCF11-IPA
I
Cytoplasm
Nucleus
Steady State mRNA
100%
50%
0%
shRNAs
Control
YTHDC1/2
ALKBH5-1
ALKBH5-2
CCDC71-IPA
J
Nuc
Cyto
63kDa
48
48
35
ALKBH5
Tubulin
ALY

Lee_Fig5

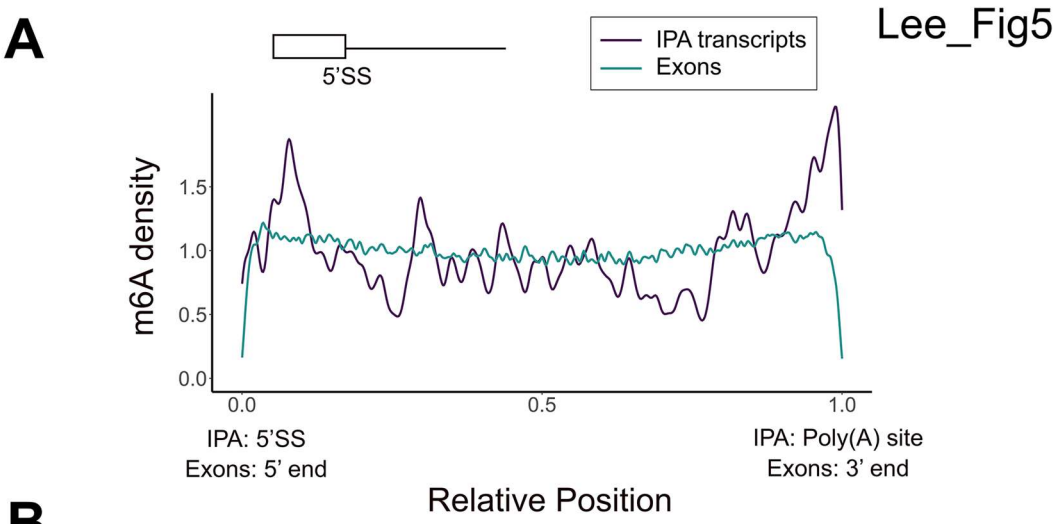
A
5'SS
IPA transcripts
Exons
m6A density
1.5
1.0
0.5
0.0
0.0
0.5
1.0
IPA: 5'SS
Exons: 5' end
IPA: Poly(A) site
Exons: 3' end
Relative Position

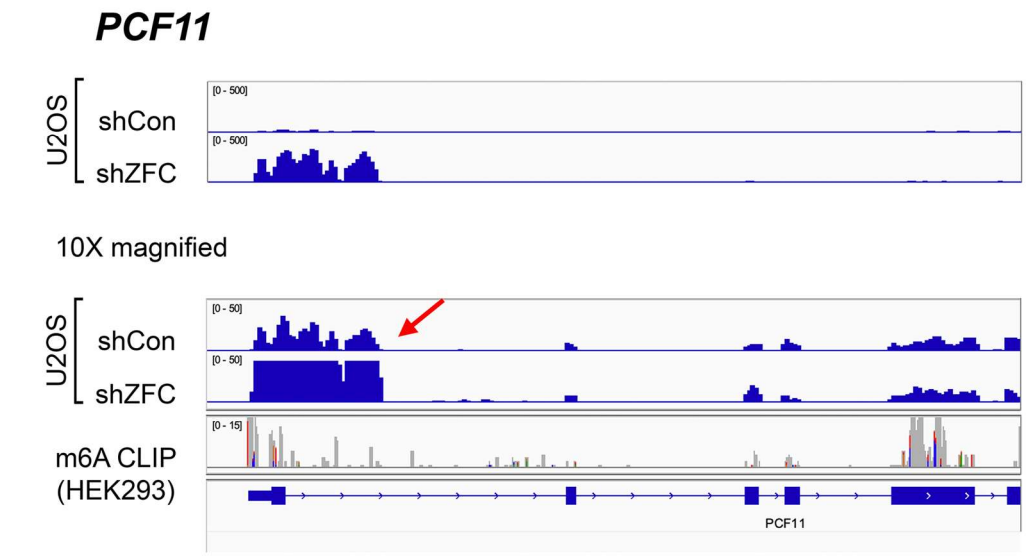
B
PCF11
U2OS
shCon
shZFC
[0 - 500]
[0 - 500]
10X magnified
U2OS
shCon
shZFC
[0 - 50]
[0 - 50]
m6A CLIP
(HEK293)
[0 - 15]
PCF11

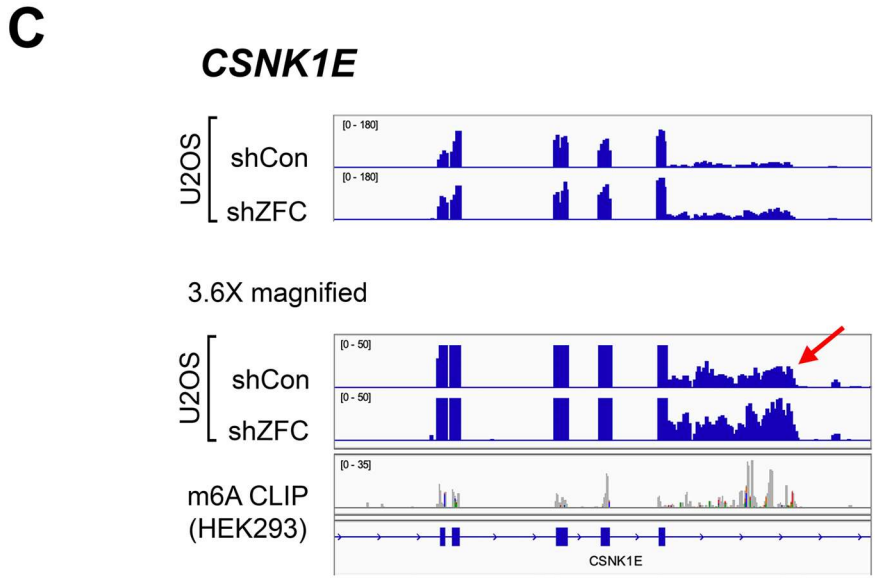
C
CSNK1E
U2OS
shCon
shZFC
[0 - 180]
[0 - 180]
3.6X magnified
U2OS
shCon
shZFC
[0 - 50]
[0 - 50]
m6A CLIP
(HEK293)
[0 - 35]
CSNK1E

Lee_Fig6

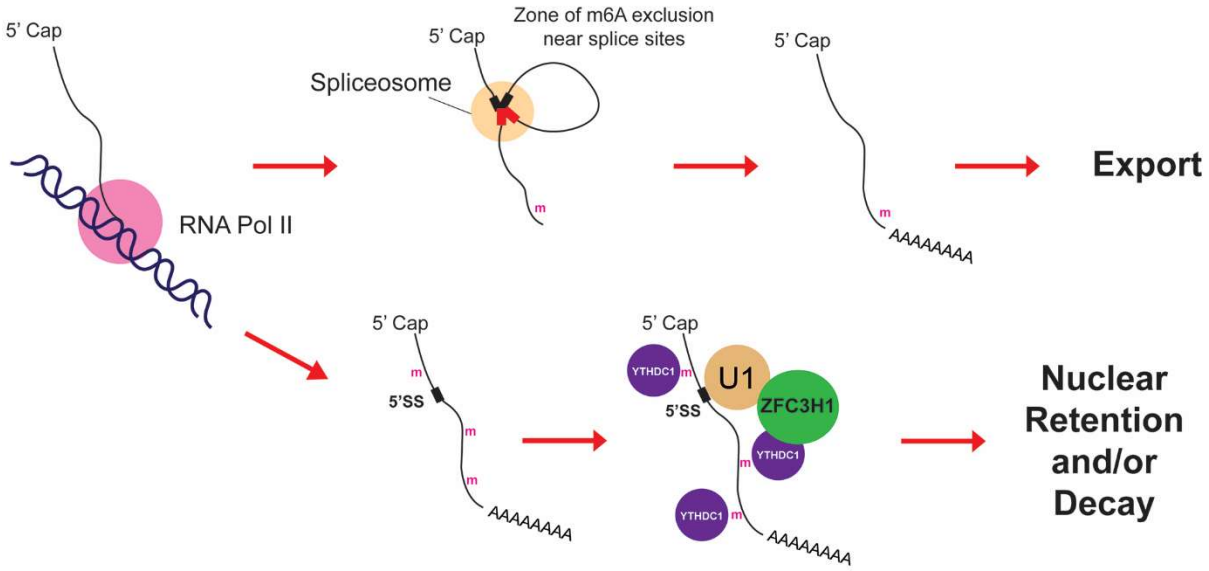
5' Cap
RNA Pol II
Spliceosome
5' Cap
Zone of m6A exclusion
near splice sites
m
5' Cap
m
AAAAAAAA
Export
5' Cap
m
5'SS
m
m
AAAAAAAA
5' Cap
YTHDC1
m
U1
5'SS
ZFC3H1
YTHDC1
m
YTHDC1
m
AAAAAAAA
Nuclear
Retention
and/or
Decay